Neuron
Article

Microcircuits of Functionally Identified Neurons in the Rat Medial Entorhinal Cortex

Andrea Burgalossi,[1,*] Lucas Herfst,[1,3] Moritz von Heimendahl,[1] Henning Förste,[2,4] Kurt Haskic,[2] Martin Schmidt,[2] and Michael Brecht[1,*]
[1]Bernstein Center for Computational Neuroscience, Humboldt University of Berlin, Philippstr. 13 Haus 6, 10115 Berlin, Germany
[2]Institut für Konstruktion, Mikro- und Medizintechnik, Fachgebiet Mikro- und Feingeräte, Technische Universität Berlin, Hardenbergstr. 36, Sekretariat EW1-2,10623 Berlin, Germany
[3]Present address: Department of Urology, Maastricht University Medical Centre, POB 5800, P. Debeyelaan 25, 6202 AZ Maastricht, The Netherlands
[4]Present address: Optris GmbH, Ferdinand-Buisson-Str. 14, 13127 Berlin, Germany
*Correspondence: andrea.burgalossi@bccn-berlin.de (A.B.), michael.brecht@bccn-berlin.de (M.B.)
DOI 10.1016/j.neuron.2011.04.003

SUMMARY

Extracellular recordings have elucidated spatial neural representations without identifying underlying microcircuits. We labeled neurons juxtacellularly in medial entorhinal cortex of freely moving rats with a friction-based, pipette-stabilization system. In a linear maze novel to the animals, spatial firing of superficial layer neurons was reminiscent of grid cell activity. Layer 2 stellate cells showed stronger theta modulation than layer 3 neurons, and both fired during the ascending phase of field potential theta. Deep-layer neurons showed little or no activity. Layer 2 stellate cells resided in hundreds of small patches. At the dorsomedial entorhinal border, we identified larger (putative parasubicular) patches, which contained polarized head-direction selective neurons firing during the descending theta phase. Three axon systems interconnected patches: centrifugal axons from superficial cells to single large patches, centripetal axons from large-patch cells to single small patches, and circumcurrent axons interconnecting large patches. Our microcircuit analysis during behavior reveals modularity of entorhinal processing.

INTRODUCTION

Understanding how cognitive functions map onto neural circuits is a fundamental goal of neuroscience. For most cognitive operations this goal is not within reach, but in rodent spatial cognition there have been three impressive advances. First, physiological studies on hippocampal and parahippocampal neurons have revealed rich and abstract representations of space. In particular, earlier studies identified place cells in the hippocampus (O'Keefe and Dostrovsky, 1971) and head-direction cells in the anterior thalamus (Taube and Muller, 1998) and the presubiculum (Taube et al., 1990a, 1990b; for a review, see Taube, 2007). Moreover, in the medial entorhinal cortex, grid cells with tessellating spatial discharges (Hafting et al., 2005), head-direction cells (Sargolini et al., 2006), and border cells (Solstad et al., 2008) have been described. Second, the large-scale anatomy of the hippocampal and parahippocampal regions is well described (van Strien et al., 2009; Suzuki and Amaral, 2004). Superficial entorhinal layers project to the hippocampal formation, whereas deep layers receive hippocampal feedback (van Strien et al., 2009). Neuronal morphologies of entorhinal cortex have been carefully characterized (Lingenhöhl and Finch, 1991; Klink and Alonso, 1997; Witter and Amaral, 2004; Quilichini et al., 2010). The architecture of medial entorhinal cortex is characterized by clusters of neurons in cytochrome oxidase-rich patches in layer 2 (Klingler 1948; Hevner and Wong-Riley, 1992; Solodkin and Van Hoesen, 1996). Third, the cognitive map theory is a powerful conceptual framework relating spatial cognition to the hippocampus (O'Keefe and Nadel, 1978) and parahippocampal regions (O'Keefe and Burgess, 2005).

Medial entorhinal cortex is a major input-output structure of the hippocampus (Burwell 2000; Suzuki and Amaral, 2004). The coexistence of grid, head-direction, and border cells suggested that the entorhinal network might be able to integrate these signals to compute an updated metric representation of position in space (Sargolini et al., 2006; Witter and Moser, 2006; Moser and Moser, 2008; Derdikman and Moser, 2010).

Despite the key role of medial entorhinal cortex in rodent spatial cognition, we still lack a mechanistic understanding of how individual neurons contribute to spatial representations. Entorhinal microcircuits remained poorly defined because extracellular recordings fail to identify the recorded neuronal elements (Chorev et al., 2009). We therefore developed a method for recording and labeling neurons in awake behaving animals and studied the anatomical properties of functionally identified neurons in relation to the patchy architecture of medial entorhinal cortex. Our data show the existence of well-defined functional microcircuits, characterized by selective axonal interconnections between cortical patches.

RESULTS

Recording and Identification of Neurons in Freely Moving Animals

We aimed at identifying microcircuits associated with spatial representations in medial entorhinal cortex. Head-anchored whole-cell recordings (Lee et al., 2006, 2009; Epsztein et al.,

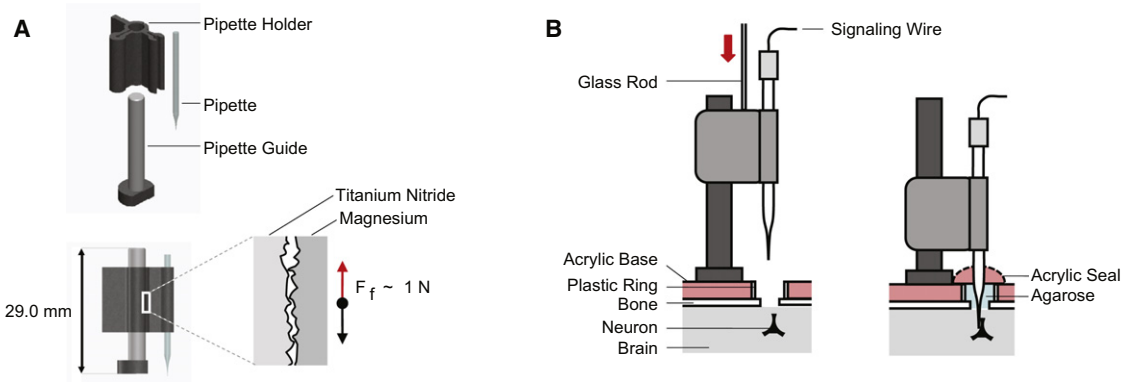

Figure 1. A Friction-Based Pipette-Positioning Device

(A) The top panel shows a disassembled pipette-positioning device. The pipette guide is implanted on the head. Bottom left is a view of an assembled pipette-positioning device; bottom right is a schematic of the friction interface between pipette holder (magnesium) and pipette guide coating (titanium nitride). The static friction force is about 1 N.

(B) The left view shows an implanted pipette-positioning device with the manipulator-driven glass rod that advanced the construct; right view shows how after staining the recorded neuron, the glass rod is pulled up, and the recording configuration is further stabilized by an acrylic seal and addition of water to the friction interface (not shown) to increase the static friction.

2010) can in principle achieve this goal, but low success rates make it difficult to recover neurons in sufficient numbers. We addressed this issue by a new method for recording and labeling neurons juxtacellularly (Pinault, 1994, 1996). A head-mountable, friction-based device held the pipette very rigidly, protecting the recording against mechanical disturbances (Figures 1A and 1B). We stabilized recordings by head anchoring the pipette with acrylic and applying water to the friction interface (Figure 1B). We worked with untrained animals that were initially anesthetized during staining and stabilization and then received an antidote against the anesthetic (Lee et al., 2006). Animals typically woke up relatively abruptly about 2–3 min after administration of the antidote and explored the maze (average distance traveled = 513 ± 462 cm; see Figures S1A and S1C available online). Because of the lack of training and perhaps also due to the wake-up procedures, animals sometimes showed only limited spatial exploration. We therefore chose to evaluate spatial firing properties not in an open field but instead in a linear "O" maze, where we typically obtained good spatial coverage of the maze (average turns = 3.9 ± 2.7). A fraction of freely moving juxtacellular recordings (~30%) was terminated deliberately to improve the rate and quality of the cell recovery (average recording length = 330 ± 316 s; see Supplemental Experimental Procedures and Figure S1B). These procedures allowed us to record spiking activity from 46 identified neurons in medial entorhinal cortex (see representative spike waveforms in Figure S1D), in 39 of which axons were visualized and traced for distances of up to 6 mm from the soma. In most recordings (65%, see Supplemental Experimental Procedures), animals sampled each location more than twice. In order to be able to judge the spatial consistency of neural activity, we restricted the assessment of spatial modulation and head-direction selectivity to this subset of recordings from identified neurons.

Large and Small Patches in Medial Entorhinal Cortex

Staining for cytochrome oxidase activity has revealed clear anatomical patterns across several brain areas, which correlated with functional neuronal activity (Wong-Riley, 1989; Wong-Riley et al., 1998). In medial entorhinal cortex, histochemical staining for cytochrome oxidase activity revealed two types of patches: "small" patches, which were restricted to layer 2; and "large" patches (Figures 2A and 2B) at the dorsal and medial borders of medial entorhinal cortex.

As pointed out in detail in the Discussion, the large patches at the medial border of medial entorhinal cortex correspond to what has been classically referred to as the superficial layers of the parasubiculum (Caballero-Bleda and Witter, 1993). The large patches at the dorsal border of medial entorhinal cortex, however, seem to not have been fully identified in previous studies (Witter and Amaral, 2004; Boccara et al., 2010). Since the medial and dorsal large patches are continuous and cytoarchitectonically similar, we consider them to be one—putatively parasubicular—structure and refer to them as large patches.

Often but not always the large patches could be divided in two vertically split subpatches (Figures 2A and 2B). Quantification of cytochrome oxidase activity levels revealed a clear periodicity of patches (Figures S2A and S2B), which were visible along the entire mediolateral extent of medial entorhinal cortex (Figures S2C–S2E).

To further characterize the organization of medial entorhinal cortex, we stained alternating parasagittal, horizontal, or tangential sections for cytochrome oxidase activity, Nissl, and myelin. Differences in cell size, density, soma morphology, and cytochrome oxidase activity confirmed the existence of the two types of patches (Figures 2A–2C). Areas of higher cell density in layer 2, as visualized by Nissl staining, coincided with the patches identified by cytochrome oxidase activity staining (Figure 2C), and the patchy organization was typically more obvious in cytochrome oxidase than in Nissl stains.

Large patches showed strong cytochrome oxidase reactivity, probably reflecting a constitutively high metabolic activity. They differed strikingly from the surrounding cortical sheet and

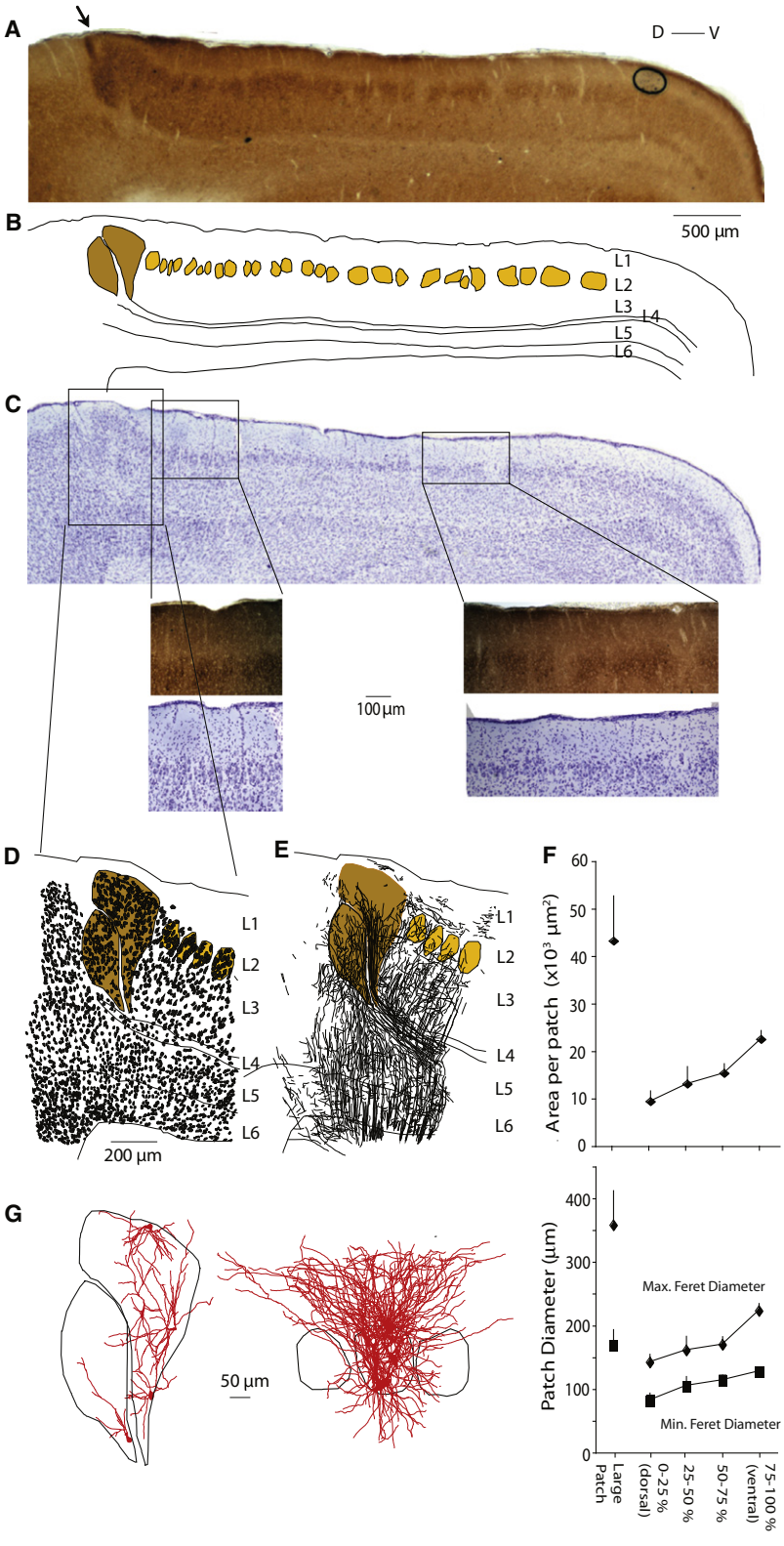

Figure 2. Small and Large Patches in Medial Entorhinal Cortex

(A) Cytochrome oxidase activity staining of a parasagittal section showing small patches in layer 2 and the large patch at the dorsal-most border of medial entorhinal cortex (indicated by the arrow). D, dorsal; V, ventral.

(B) Drawing of layers, small layer 2 patches (light brown), and the pair of large patches (dark brown) from the section shown in (A).

(C) Top view shows parasagittal section adjacent to (A) stained for Nissl substance. Bottom views illustrate high magnification of the boxes indicated above with the corresponding cytochrome oxidase activity stains from the section in (A).

(D) Drawing of neuronal somata (black) revealed by a Nissl stain in the parasagittal section of the dorsal border of medial entorhinal cortex shown in (C). Outlines of cytochrome oxidase patches recognized in the adjacent section (A) are superimposed for clarity.

(E) Drawing of myelinated axons (black) revealed by a myelin staining with superimposed cytochrome oxidase activity staining pattern from an adjacent section.

(F) Top view shows quantification of patch area along the dorsoventral axis. Bottom view illustrates quantification of maximal and minimal Feret diameters (maximal diameter corresponding to the longest dimension across all orientations and minimal diameter corresponding to that of the smallest inscribed circle) of patches along the dorsoventral axis. Data are from five different brains (bins of 25%; 100% = maximal axis length; see Figure S3). Error bars indicate standard error.

(G) Reconstructions of dendritic morphologies from five neurons recovered from large patches (left) and seven layer 2 stellate neurons (right) superimposed on the outline of the patches. Care was taken to correctly position the reconstructions relative to the border nearest to the soma and to position the reconstructions such that the relative position of the cell in its patch is reflected in the superposition. Note the strong polarization of large patch cells away from patch borders. Dendrites from layer 2 stellate cells were also largely (though not perfectly) restricted to their home patch within layer 2. See also Figure S4.

distorted the cortical lamination (Figure 2D). Their broad dorsal part extended into layer 1, and their ventral part tapered out toward layer 4. Many myelinated axons originated from these patches, but myelination did not extend into their broad dorsal part (Figure 2E). The small layer 2 patches were also often surrounded by myelinated fibers (data not shown). The architecture of small patches changed along the dorsoventral axis: cell size and myelination decreased (data not shown), while patch size increased (Figure 2F; Figure S3). Cells in large patches appeared to be smaller than adjacent neurons in small layer 2 patches (Figure 2D) and had a unique dendritic morphology, strongly polarized away from the patch border (Figure 2G). Within layer 2 the dendrites of layer 2 stellate cells were also largely but not exclusively restricted to their home patch, while they extended more broadly in layer 1 (Figure 2G; Figure S4). Interestingly, patch diameters seemed to be within the range of the deep-to-superficial "input clusters" widths reported by

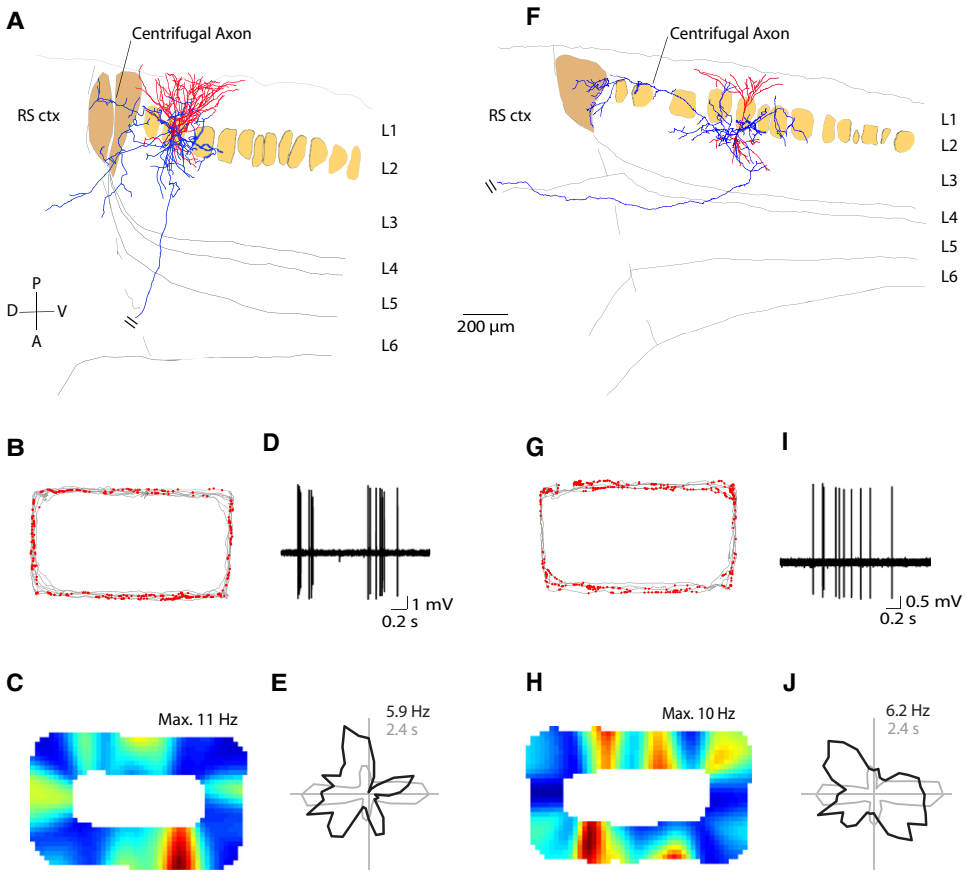

Figure 3. Identified Neurons from the Superficial Layers of Medial Entorhinal Cortex

(A) Reconstruction of the dendritic (red) and axonal (blue) morphology of a layer 2 spiny stellate neuron with a superimposed outline of cytochrome oxidase activity stain that identified small layer 2 (light brown) and a pair of large patches (dark brown) in this parasagittal section. Centrifugal axonal projection is indicated. The dashed line demarcates the border of medial entorhinal cortex with retrosplenial cortex (RS ctx). D, dorsal; V, ventral; A, anterior; P, posterior.

(B) Firing locations of spikes (red) and trajectory of the rat (gray) during running in clockwise direction in a 120 × 60 cm "O"-shaped maze.

(C) Color-coded rate map for the spikes in (B) (bins of 2.5 × 2.5 cm, maximum firing rate indicated above).

(D) High-pass filtered spike trace recorded during freely moving behavior.

(E) Firing rate (black) and occupancy times (gray) as a function of head direction. Peak firing rate and minimum occupancy time are indicated.

(F–J) Recording from a layer 3 pyramidal neuron. Conventions are the same in (A)/(F), (B)/(G), (C)/(H), (D)/(I), and (E)/(J), respectively. Scale bar is the same for (A) and (F). Axon thickness has been increased for display purposes. Note that both neurons displayed multiple spatially separated firing peaks.

The discharge pattern of the neurons in individual laps is shown in Figure S5.

Beed et al. (2010) for stellate cells (~200 µm at midlevel of medial entorhinal cortex), suggesting a possible correlation between patches and interlaminar inputs in medial entorhinal cortex.

Spatial Firing Behavior of Superficial Neurons

Next, we studied the response properties of identified neurons in medial entorhinal cortex while the rat explored a novel environment. Moreover, to relate neuronal morphology to the patchy cortical organization, we double stained brain sections for biocytin and cytochrome oxidase activity.

A recording experiment from a layer 2 spiny stellate cell is shown in Figures 3A–3E. Staining for cytochrome oxidase activity revealed that the neuron was located in a small layer 2 patch (Figure 3A). In layer 2, axon and dendrites were largely but not completely restricted to the patch, whereas dendrites extended beyond the territory above the patch in layer 1. A descending axon and several long axon collaterals could be identified (Figure 3A). One of these collaterals targeted a large patch; as this collateral ran from the inner part of medial entorhinal cortex to its border, we refer to it as the "centrifugal" axon. This cell showed multiple spatially separated firing peaks (Figures 3B and 3C), a firing behavior similar to grid cells in linear environments (Hafting et al., 2008; Brun et al., 2008; Mizuseki et al., 2009). This neuron discharged in bursts whose occurrence was often modulated at the theta frequency (Figure 3D). In four out of four layer 2 neurons where spatial modulation of activity could be assessed (see Supplemental Experimental Procedures), we observed multiple spatial firing peaks. Head-direction tuning was measured as the normalized average vector of the circular distribution of firing rates (see Experimental Procedures). This neuron showed little or no head-direction selectivity (head-direction index = 0.24; Figure 3E).

Figures 3F–3J show a recording of a spiny layer 3 pyramidal cell (Figure 3F). The dendrites arborized in layer 1 and 3 with few dendritic segments extending in layer 2. Also in this cell, a centrifugal axon collateral targeted a large patch. This cell showed multiple spatially separated firing peaks reminiscent of grid cells (Figures 3G and 3H). Consistent with previous work (Hafting et al., 2005; Sargolini et al., 2006), a fraction of layer 3 cells (four out of nine) showed a similar spatial activity pattern. The neuron's spike discharges were regular and not modulated at the theta frequency (Figure 3I). This neuron showed little selectivity for head direction (head-direction index = 0.05; Figure 3J).

Several observations indicate that the multiple firing peaks observed in the linear maze reflected a consistent spatial modulation. First, when we plotted individual laps of the recorded neurons, we found spatially repeating firing peaks in 8 out of 13 layer 2/3 recordings, which qualified for spatial modulation analysis (see Supplemental Experimental Procedures and Figures S5A–S5C). Second, repeating firing fields occupied only a small part of the arena (cumulative area <30%; see Figure S5E), suggesting that firing was spatially restricted. Third, the strong firing rate modulation observed in averaged rate maps (Figure S5F) together with the rare occurrence of single-lap firing fields (Figure S5E) reinforces the observation that firing was spatially consistent (Figures S5A–S5C).

To quantify spatial consistency, we ranked cells according to the extent to which firing repeated in restricted spatial locations. To this end, we computed the fraction of repeating firing fields (as opposed to single-lap firing fields) divided by the area they covered (see Supplemental Experimental Procedures). In two layer 2 neurons, this ratio was larger than 5, in accordance with a striking, spatially restricted firing pattern. In the case shown in Figure S5A, one firing field was present in four out five laps, another one in three out five laps, and only little other activity was observed. In six further recordings this ratio (fraction of repeating firing fields divided by the area they covered) was between 2 and 4, with most though not all firing fields appearing in multiple laps (Figures S5B and S5C). In the remaining five cells, this ratio was <2, and they did not show spatially consistent firing activity (Figure S5D). These findings are consistent with the conclusions of other authors (see Moser and Moser, 2008 for review) that a large fraction of cells in medial entorhinal cortex are spatially modulated. Given the limited duration of our recordings, however, our assessment of spatial consistency remains preliminary.

We labeled 21 spiny, putatively excitatory, neurons in superficial layers (nine layer 2, 11 layer 3; one cell was located at the layer 2/3 border and was not included in the functional analysis). A large fraction of layer 2 cells could be classified as stellate (eight out of nine) and in layer 3 as pyramidal neurons (all eight cells that had complete dendritic morphology), confirming previous work (Lingenhöhl and Finch, 1991; Klink and Alonso, 1997). We observed a centrifugal axon in 15 out of 18 superficial layer cells with a well-filled axon. This projection was highly selective with axons traveling for long distances to branch in single large patches.

Deep-Layer Neurons Are Largely Silent

Figures 4A–4E show a recording experiment from a layer 5 pyramidal cell (Figure 4A) with dendrites in the deep layers and an apical dendrite extending toward the pia without an elaborate tuft. The axon arborized extensively in layers 3–6, and a single descending axon collateral was identified (Figure 4A). The neuron showed very little activity during exploration but became slightly more active during resting (Figures 4B–4E). Given the low level of activity and the bias of spiking toward resting, it remained unclear if the discharge pattern reflected a true spatial modulation (Figures 4B and 4C) or head-direction selectivity.

Figures 4F–4J show a recording of a spiny layer 6 multipolar cell with long thin dendrites and an axon that extended within deep layers (Figure 4F). Much like the layer 5 cell described above, this layer 6 neuron showed very little activity and became more active during rest (Figures 4G–4J). Because the firing rate was very low, spatial modulation and head-direction selectivity could not be assessed in a meaningful way.

The 11 neurons recovered from deep layers (eight layer 5, three layer 6) showed remarkably low levels of activity. Five out of 11 cells were completely silent, and the presence of these cells in the awake animal could only be verified by juxtacellular current injection (see Supplemental Experimental Procedures). Even though in eight cells long axons were identified, we did not observe any centrifugal axon. Thus, the large patches receive inputs from superficial but not from deep layers.

Head-Direction Selectivity and Microcircuits of Neurons in the Large Dorsal Patches

The selective axonal projection to large patches prompted us to characterize these structures. Prior to juxtacellular labeling, we identified large patches at the dorsal-most border of medial entorhinal cortex through extracellular recordings in awake head-fixed animals. The large patches could be located by a sudden increase in field theta activity (see also Fyhn et al., 2008).

Figures 5 and 6 show recordings from large patch neurons. The morphology of the identified neurons was different from cells in the rest of medial entorhinal cortex. Dendritic arbors were often small and restricted to the home patch. Axons arborized locally and sent out a descending axon and two additional long-range collaterals (Figures 5A, 5B, 6A, 6B, 6G, and 6H). As best visualized in the projection of the reconstructed neuron onto a tangential plane (Figures 5B, 6B, and 6H), one collateral connected to many other large patches; we refer to this collateral as the ''circumcurrent'' axon as it ran mediolaterally along the border of entorhinal cortex. A second collateral targeted specifically (i.e., without branches) one or two small layer 2 patches and arborized within these structures. As this collateral ran from the border of medial entorhinal cortex to its inner part, we refer to it as ''centripetal'' axon.

Some neurons were spatially broadly tuned (Figures 5C–5E, 6I, and 6J), while others showed a multipeaked firing behavior (Figures 6C and 6D). Neurons in the large patches had two striking physiological characteristics. First, spike discharges were typically strongly modulated in the theta frequency range (Figures 6E and 6K). Second, compared to superficial layer cells, these neurons displayed higher degrees of head-direction tuning (head-direction index = 0.39, Figure 5F; head-direction index = 0.38, Figure 6F; head-direction index = 0.77, Figure 6L).

In a linear environment an artifactual impression of head-direction selectivity could arise if an animal traversed the maze only in

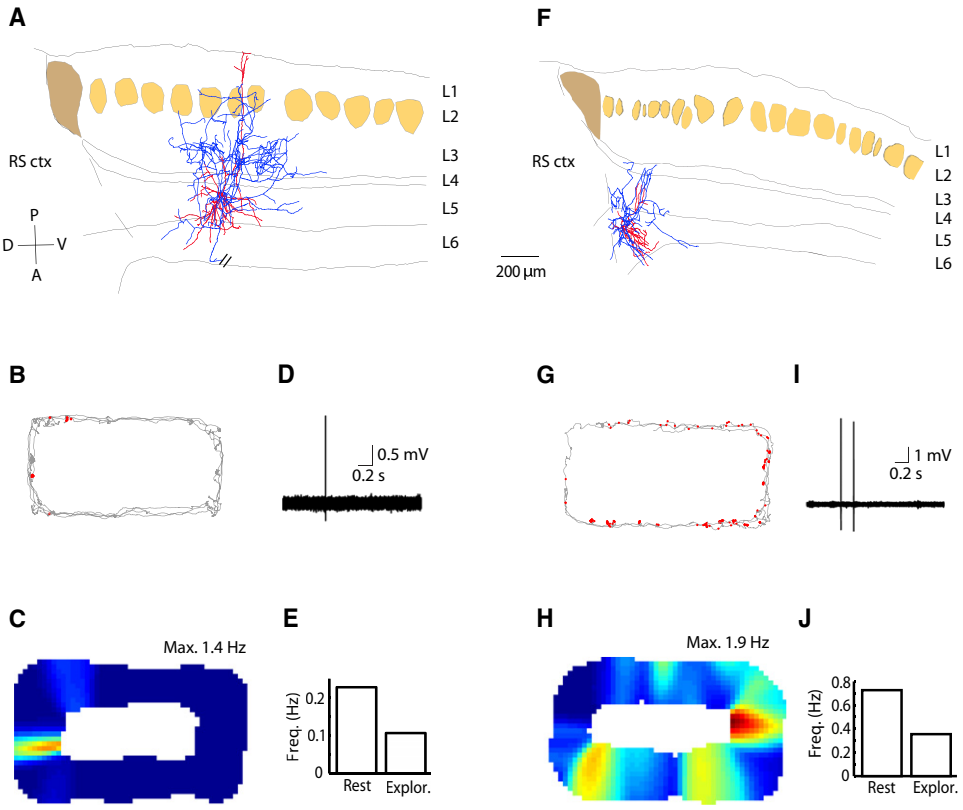

Figure 4. Identified Neurons from the Deep Layers of Medial Entorhinal Cortex

(A) Reconstruction of the dendritic (red) and axonal (blue) morphology of a layer 5 pyramidal neuron with a superimposed outline of cytochrome oxidase activity stain that identified small layer 2 (light brown) and large patches (dark brown) in this parasagittal section. The dashed line demarcates the border of medial entorhinal cortex with retrosplenial cortex (RS ctx). D, dorsal; V, ventral; A, anterior; P, posterior.

(B) Firing locations of spikes (red) and trajectory of the rat (gray) during running in clockwise direction in a 120 × 60 cm "O"-shaped maze.

(C) Color-coded rate map for the spikes in (B) (bins of 2.5 × 2.5 cm, peak firing rate indicated above).

(D) High-pass filtered spike trace recorded during freely moving behavior.

(E) Averaged activity during exploration and rest (defined as periods without locomotion).

(F–J) Recording from a layer 6 multipolar neuron. Conventions are the same in (A)/(F), (B)/(G), (C)/(H), (D)/(I), and (E)/(J), respectively. Scale bar is the same for (A) and (F). Axon thickness has been increased for display purposes. These neurons displayed higher activity during rest than while exploring the environment.

one direction and the cell's firing was restricted to one arm of the maze. Several lines of evidence indicate, however, that such an explanation does not account for the head-direction selectivity observed in large patch cells: (1) firing of both large patch cells (Figures 5 and 6) and other entorhinal neurons (Figure 3) was typically not restricted to single arms of the maze; (2) firing varied at single locations as a function of head direction; and (3) in three dorsal patch cells, where we sampled sufficient data from both clockwise and counterclockwise running directions, firing locations jumped as a function of running direction (Figure S6; see Figures 6I and 6J for an example), suggesting that these neurons carry directional rather than positional information.

The 14 neurons recovered from large patches formed very similar microcircuits. In 10 out of 12 cells with a well-filled axon, we observed both circumcurrent and centripetal axons; in the remaining two only a circumcurrent axon was observed. In three neurons from large patches, we could follow a descending axon subcortically and observed branching in the presubiculum (data not shown).

Response Properties and Discharge Timing Differ across Layers and Patches

We summarize the striking physiological differences between the entorhinal layers and patches in Figure 7; Figure S7. Cells in layers 2 and 3 and the large patches were active during exploration, whereas deep layers showed little spiking activity (Figure 7A). Under our experimental conditions, head-direction selectivity was weak in layers 2 and 3, and low activity levels prevented the assessment of head-direction selectivity in deep layers. The strongest head-directional modulation of firing was observed from the population of large patch neurons (Figure 7B).

Neurons in different entorhinal compartments showed pronounced differences in their temporal discharge patterns. To examine the spike timing relative to the theta rhythm, we obtained the phase of the theta oscillation from the field potential signal, which we extracted from our juxtacellular recordings (Figures 7C–7E). On average, firing of the layer 3 cell population was biased toward the ascending phase of the theta cycle (Figures 7F and 7G; Rayleigh average vector length = 0.092 and

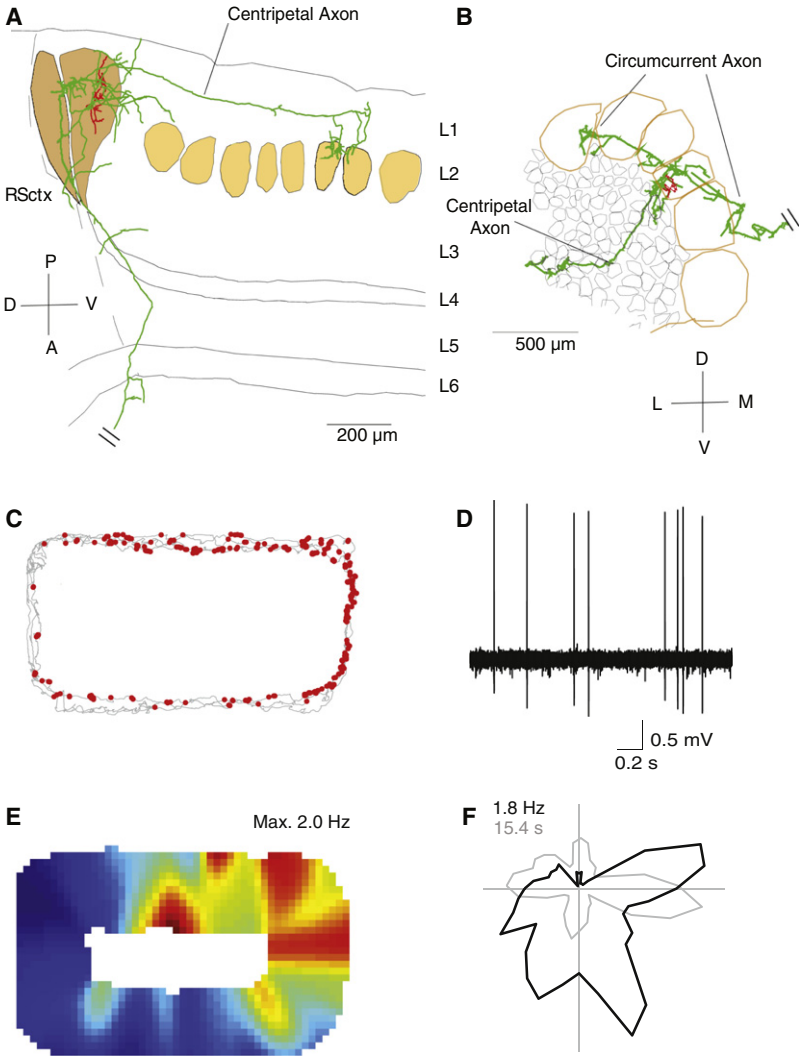

Figure 5. Identified Neuron from a Large Patch

(A) Reconstruction of the dendritic (red) and axonal (green) morphology of a cell recorded from a large patch with a superimposed outline of cytochrome oxidase activity stain that identified small layer 2 (light brown) and large patches (dark brown) in this parasagittal section. The centripetal axonal projection is indicated. The dashed line demarcates the border of medial entorhinal cortex with retrosplenial cortex (RS ctx). D, dorsal; V, ventral; A, anterior; P, posterior.

(B) Projection of the reconstructed neuron onto a tangential plane. For display purposes, the neuron is shown superimposed on a reconstruction of small layer 2 (black) and large patches (brown) from a myelin stain of a tangential section (prepared from another animal as described in the Supplemental Experimental Procedures). Care has been taken in the superposition to correctly align the reconstruction with respect to large and small patches. Axon thickness has been increased for display purposes. The circumcurrent and centrifugal axonal projections are indicated. Same conventions as in (A). D, dorsal; V, ventral; M, medial; L, lateral.

(C) Firing locations of spikes (red) and trajectory of the rat (gray) during running in clockwise direction in a 120 × 60 cm "O"-shaped maze.

(D) Representative high-pass filtered spike trace recorded during freely moving behavior.

(E) Color-coded rate map for the spikes in (C) (bins of 2.5 × 2.5 cm, maximum firing rate indicated above). This cell displayed broadly distributed spatial activity.

(F) Firing rate (black) and occupancy times (gray) as a function of head direction. Peak firing and minimum occupancy time are indicated.

greater than expected by chance; $p < 0.002$), with weak phase locking to the field potential theta (Figure S7A). Individual layer 2 cells showed stronger theta-phase locking (Figure S7A) and on average tended to fire preferentially on the ascending phase of the theta cycle (Figure 7G), in agreement with recent observations (Hafting et al., 2008). However, theta-phase preferences in layer 2 were heterogeneous (Figure 7F; Figure S7A; Rayleigh vector not significant; $p = 0.615$). It appears that this heterogeneity of theta-phase preferences might be at least in part accounted for by the laminar location of the tip of the recording pipette, which we could identify in all of our recordings. The polarity of the field potential theta signal is known to invert on the pial side of layer 2 (Alonso and García-Austt, 1987; Chrobak and Buzsáki, 1998; Hafting et al., 2008; Mizuseki et al., 2009) (Figure S7A). In all recordings from superficial layer neurons in which we observed firing preferences on the ascending phase of the theta cycle, recording locations were well within layers 2 and 3. However, in two out of eight recordings from layer 2 cells, in which we observed preferences on the descending theta phase, it appeared that the recording pipette tip was located in layer 1 (Figure S7A). Interestingly, large patch cells showed the strongest theta-phase locking (Figures 7F and 7G; Rayleigh average vector length = 0.35; $p < 0.003$) and in contrast to superficial neurons, showed maximal firing on the descending phase of the theta cycle, near the trough (difference in average vector angle: layer 2 versus large patch = 170°, $p = 0.006$; layer 3 versus large patch = 167°, $p = 0.004$) (Figures 7F and 7G; Figure S7A).

Autocorrelation analysis indicated that theta modulation of activity was strong in layer 2 and weak in layer 3 cells (Figures S7A and S7B), consistent with differences of oscillatory discharge behavior described in vitro (Alonso and Klink, 1993; van der Linden and Lopes da Silva, 1998). In line with the strong theta modulation of the field potentials, the largest fraction of theta-modulated cells was found in large patches (Figure S7B).

Large-Scale Axonal Organization of Patches

In order to explore the axonal connectivity scheme across medial entorhinal cortex, we visualized the large-scale architecture of axons traveling in layer 1 in "mass" myelin stains of tangential sections (Figure 8). Large patches (dark brown) were identified by cell somata clustering and by the clear myelination pattern that surrounded these structures (Figure S8). Figure S8, which shows serial sections through the dorsomedial part of medial entorhinal cortex, also illustrates that large patches seemed to

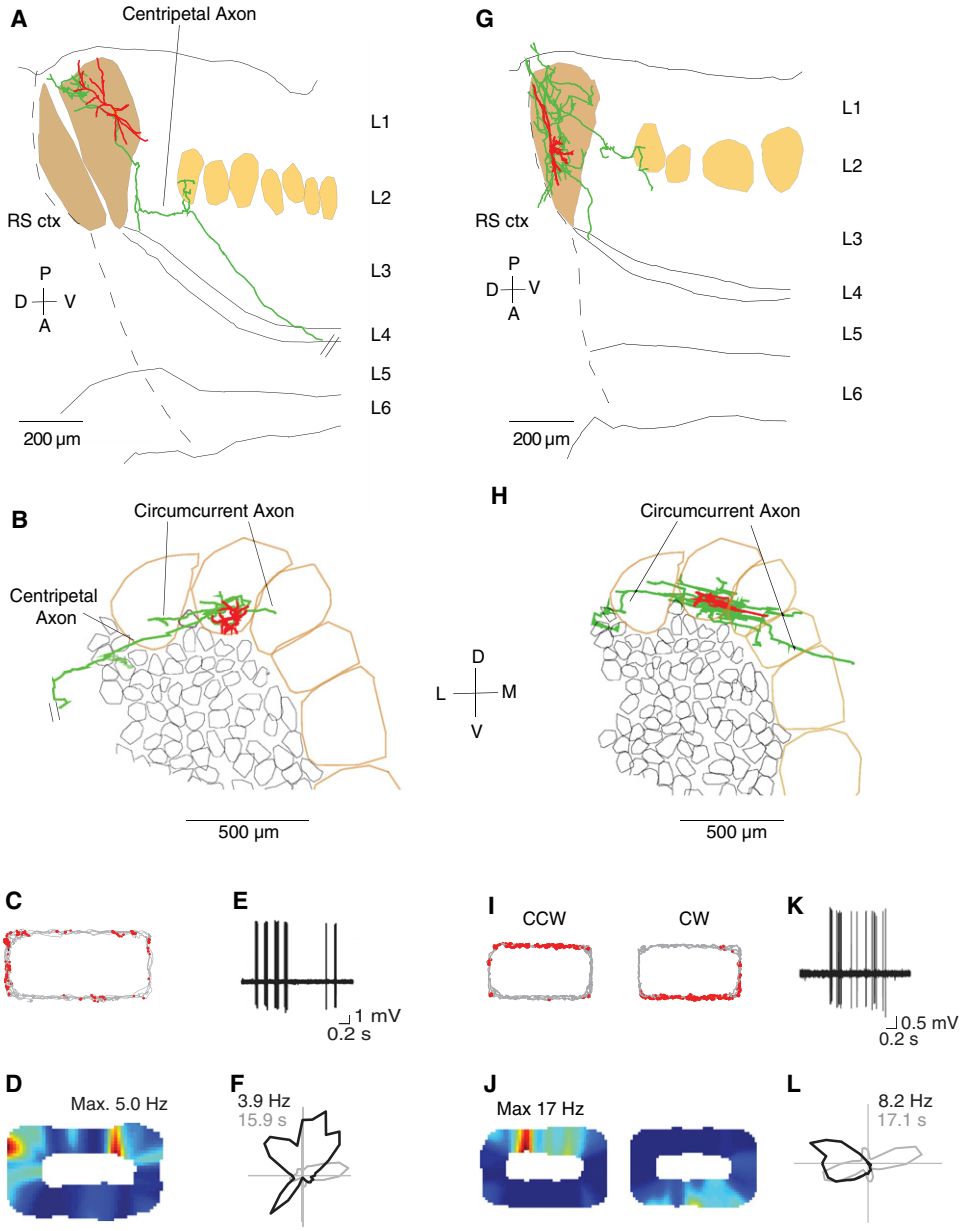

Figure 6. Head-Direction Selectivity and Microcircuits of Neurons in the Large Patches

(A) Reconstruction of the dendritic (red) and axonal (green) morphology of a cell recorded from a large patch with a superimposed outline of cytochrome oxidase activity stain that identified small layer 2 (light brown) and large patches (dark brown) in this parasagittal section. The centripetal axonal projection is indicated. The dashed line demarcates the border of medial entorhinal cortex with retrosplenial cortex (RS ctx). D, dorsal; V, ventral; A, anterior; P, posterior.

(B) Projection of the reconstructed neuron onto a tangential plane. For display purposes, the reconstruction is shown superimposed on a myelin stain from a tangential section (prepared from another animal) that shows small layer 2 (black) and large patches (brown). Care has been taken in the superposition to correctly align the reconstruction with respect to large and small patches. Axon thickness has been increased for display purposes. The circumcurrent and centripetal axonal projections are indicated. Same conventions as in (A). D, dorsal; V, ventral; M, medial; L, lateral.

(C) Firing locations of spikes (red) and trajectory of the rat (gray) during running in clockwise direction in a 120 × 60 cm "O"-shaped maze.

(D) Color-coded rate maps for the spikes in (C) (bins of 2.5 × 2.5 cm, maximum firing rate indicated above).

(E) Representative high-pass filtered spike trace recorded during freely moving behavior.

(F) Firing rate (black) and occupancy times (gray) as a function of head direction. Head-direction selectivity was computed for the entire recording trial, including both clockwise (C) and counterclockwise (not shown) running directions. Peak firing rate and minimum occupancy time are indicated.

(G–L) Conventions are the same in (A)/(G), (B)/(H), (C)/(I), (D)/(J), (E)/(K),and (F)/(L), respectively. Note that in this cell only a circumcurrent axon was identified (H). Firing locations of spikes (I) and color-coded rate maps (J) are shown separately for clockwise (CW) and counterclockwise (CCW) running directions.

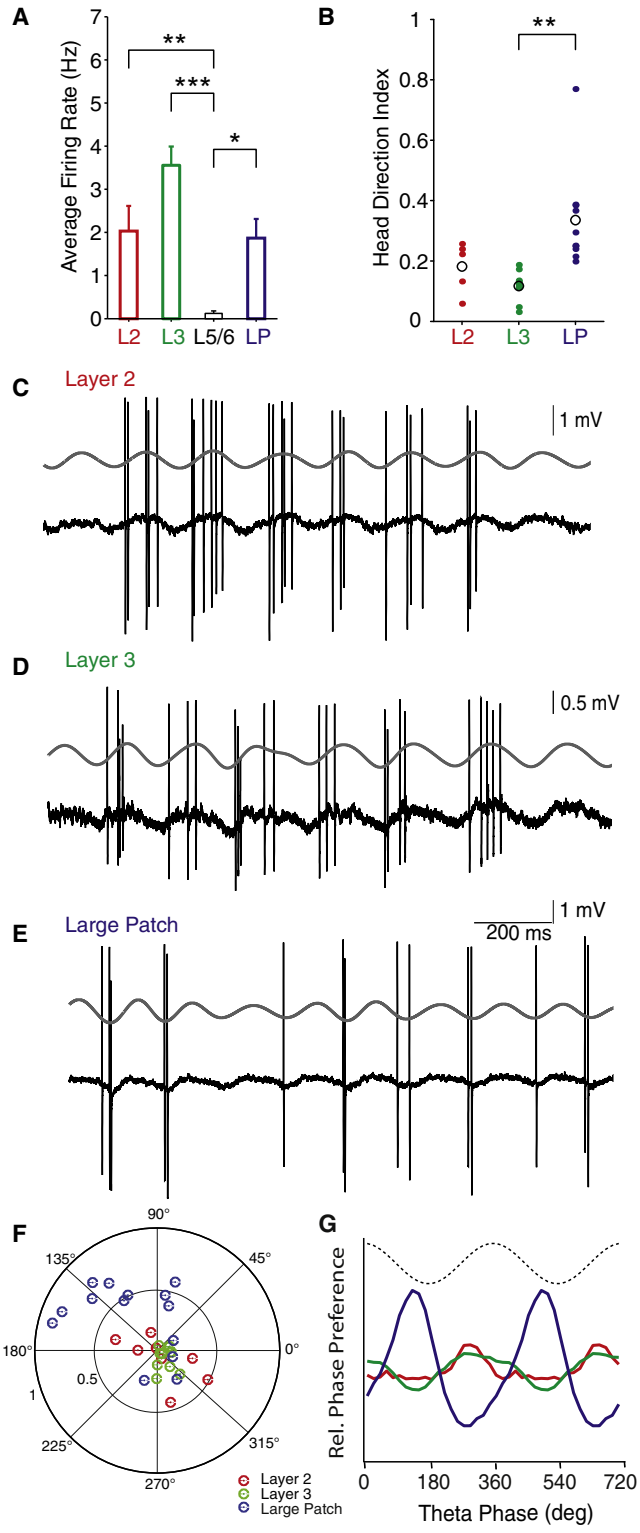

Figure 7. Response Properties across Layers and Patches

(A) Average firing rates for all recorded cells in layer 2 (L2, n = 9; one neuron was silent), layer 3 (L3, n = 11), layer 5-6 (L5-6, n = 11; five neurons were silent), and large patches (LP, n = 14). Error bars indicate standard error. Average firing rates differed significantly between L5-6 and every other group.

(B) Head-direction index for cells in L2 (n = 5), L3 (n = 10), and LP (n = 10). Head-direction tuning was quantified as the normalized average vector of the circular distribution of firing rate. L3 and LP differed significantly. Circles indicate mean values. One (*), two (**), and three (***) asterisks indicate significance at the 0.05, 0.01, and 0.001 levels, respectively.

(C–E) Representative raw spike traces (black, bottom) recorded for layer 2 (C), layer 3 (D), and large patch cells (E) during 1.5 s of running behavior. Superimposed on top (gray) is the band-pass filtered (4–10 Hz) field potential trace. The amplitude of the filtered trace has been increased 2-fold for display purposes. Note the differences in spike timing between layer 2/3 and large patch neurons.

(F) Polar plots of layer 2 (red), layer 3 (green), and large patch cells (blue) representing both the preferred phase (peak = 0°, 360°; trough = 180°) and the modulation strength (average vector, proportional to the distance from the center) for each single neuron.

(G) Relative phase preference for layer 2, layer 3, and large patch cells. The phase of the theta cycle is shown above (dotted line). Two cycles are shown. Note the difference in phase preferences of large patch cells compared to superficial layer neurons. Colors as in (F).

form a *continuum* with the parasubiculum (Shipley, 1974, 1975; Köhler, 1984; Caballero-Bleda and Witter, 1993; Witter and Amaral, 2004). Myelin stainings revealed a striking regularity of layer 1 axonal fibers, organized in axonal bundles running along the dorsomedial to ventrolateral axis (Figure 8A). We traced putative centrifugal axons originating above the territory of small layer 2 patches (blue, Figures 8A and 8C), and we drew a large number of axons that surrounded a single large patch (green, Figures 8A and 8B). As in most identified cells from large patches (Figures 5 and 6), putative circumcurrent axons to dorsolateral neighboring patches were longer and more prominent than axons extending toward the ventromedial ones (green, Figures 8A and 8B). A schematic overview of the position of medial entorhinal patches in the rat brain is shown in Figure 8D. Overall, the circumcurrent axons surrounding large dorsal patches were much more numerous than the circumcurrent axons surrounding medioventral patches. Mass myelin stains appear to be consistent with our single-cell reconstruction data and suggest a global organization of three long-range axon systems in medial entorhinal cortex: (1) centrifugal and (2) centripetal axons, which reciprocally connect large and small patches; and (3) circumcurrent axons, which connect large patches along the mediolateral axis. Because mass myelin stains cannot ascertain the origin and endpoint of axonal projections, additional tracing work will be required to firmly establish the reciprocal nature of centrifugal and centripetal connections.

DISCUSSION

To our knowledge, we provided the first microcircuit description of functionally identified cells in medial entorhinal cortex. Friction-based pipette-stabilization and juxtacellular labeling allowed the combined analysis of neural activity, circuitry, and behavior. We demonstrated efficient (>50% success rates) cell recovery with excellent morphology from freely moving animals. The success of the friction-based device is almost certainly related to the rigidity of the pipette positioning. As the pipette is securely locked into position, the resulting recordings withstand mechanical disturbances. As only a handful of neurons

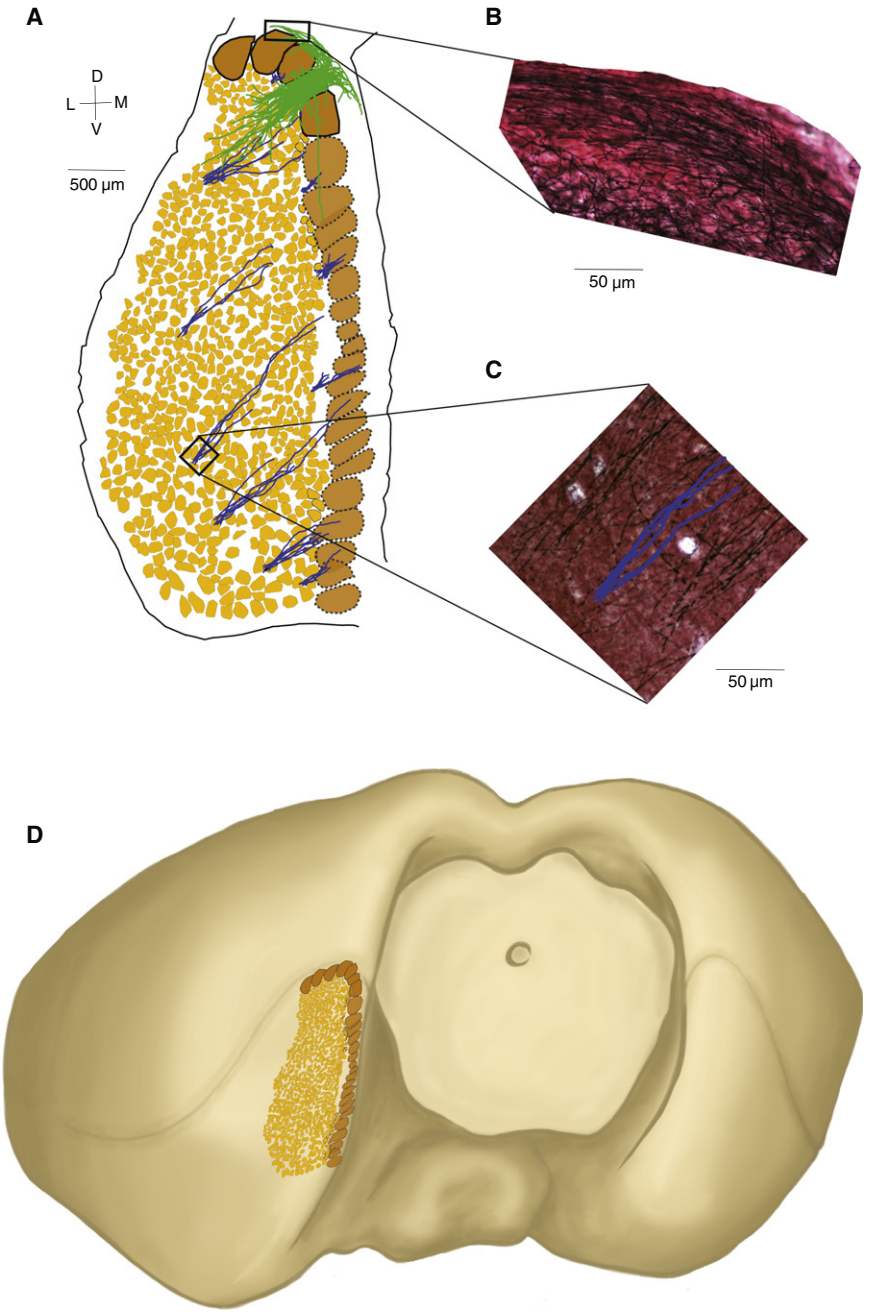

Figure 8. Large-Scale Architecture of Layer 1 Axons in Medial Entorhinal Cortex

(A) Reconstruction of the architecture of medial entorhinal cortex from serial tangential sections stained for myelin. Large patches at the dorsal-most border of medial entorhinal cortex were detected by massive axon bundles on the dorsal surface of each patch; subdivisions between pairs of patches were visible in a subset of them but are not indicated. Most of the borders of medial large patches were difficult to discern in this preparation, and their outlines have been dashed. Small layer 2 patches were detected in mid-depth of layer 2 as clusters of white somata surrounded by myelin. For consistency with other panels, we illustrate large patches in dark brown and small layer 2 patches in light brown. Layer 1 was densely populated with axon bundles, and roughly twice as many axon bundles as small patches were detected. Ten bundles originating above small patches (putative centrifugal axons; blue) and axons associated with one large patch (putative centripetal and circumcurrent axons; green) were drawn. The reconstruction was performed across twelve 40 µm sections stained for myelin. The reconstruction encompasses most but not all of medial entorhinal cortex; in particular, it appeared that small and large patches were missed laterally, probably because of the cortical curvature and their poor alignment with the sectioning angle. Note that axons could only be followed for limited distances and that axon thickness has been increased for display purposes. D, dorsal; V, ventral; M, medial; L, lateral.

(B) Myelin-stained inset showing putative circumcurrent axons. Magnification of the marked section in (A).

(C) Myelin-stained inset showing bundles of putative centrifugal axons in layer 1. Magnification of the marked section in (A).

(D) Schematic representation of the patchy organization of medial entorhinal cortex in a posterior-lateral view of the rat brain (based on the same reconstruction shown in A). To give a more complete overview, additional large and small patches have been added dorsolaterally, which were not reconstructed from the sections used for (A) because they could not be well visualized as a result of the curvature of the brain. The rhinal fissure is indicated.

have been recovered from freely moving mammals previously, our approach opens up a new frontier in microcircuit research. Beyond cell identification, our methodology provides additional advantages over conventional extracellular recording techniques. First, it allows unequivocal unit separation, given the remarkably high signal-to-noise ratio of the recorded spike signals (average signal-to-noise = 11.64 ± 6.9; see Supplemental Experimental Procedures and Figure S1D). Second, it allows recording and identifying silent cells, whose impact on cortical computations is poorly understood. Third, activity of the recorded cells can be manipulated by current injections (Houweling and Brecht., 2008; Voigt et al., 2008; Houweling et al., 2010), making it possible to explore the effects of single-cell stimulations on freely moving animal behaviors. A major limitation of the current method is the use of the antagonizable anesthesia. Although under the same conditions as the present study hippocampal physiology seemed to be preserved to a large extent (e.g., occurrence and properties of place cells were unaltered) (Lee et al., 2006, 2009; Epsztein et al., 2010), we cannot exclude potential residual effects of the anesthesia after antagonization.

In the present study we made three key observations. First, we identified two types of patches in medial entorhinal cortex: small

patches in layer 2 and large patches at the dorsomedial border. Second, we identified the connections between patches. Superficial layer cells connect to single large patches (via centrifugal axons), whereas cells from these structures connect back to small patches (via centripetal axons) and to other large patches (via circumcurrent axons). Third, we characterized the functional properties of identified cells in the different compartments of medial entorhinal cortex. Altogether, our data point to a congruence of connectivity and responses with cortical patches, implying that these units—described not only in rats but also in monkeys and humans (Hevner and Wong-Riley, 1992; Solodkin and Van Hoesen, 1996)—shape entorhinal processing in a fundamental way.

Grid cells display a periodic and regular hexagonal firing pattern while the rat explores an open field (Hafting et al., 2005). Typically, such strict periodicity of firing pattern is not observed in linear environments (Hafting et al., 2008; Brun et al., 2008; Mizuseki et al., 2009), which makes it impossible under our conditions to certify if a cell is a grid cell or not. The largest fraction of grid cells were recorded from superficial layers of medial entorhinal cortex (Hafting et al., 2005; Sargolini et al., 2006; Boccara et al., 2010). In agreement with these studies, we also observed a large fraction of cells with multipeaked firing behavior in layer 2 and 3, a firing pattern that is reminiscent of grid cells tested in linear environments (Hafting et al., 2008; Brun et al., 2008; Mizuseki et al., 2009). The spatial firing across laps was highly stable in some cells (Figure S5A) but less reproducible in other neurons (Figures S5B and S5C). The complete novelty of the environment might contribute to the instability of spatial firing, as previously suggested (Hafting et al., 2005; Langston et al., 2010; Wills et al., 2010). Finally, we cannot rule out that external, potentially uncontrolled nonspatial stimuli contributed to the observed spatial modulation because we did not perform spatial manipulations (such as cue-card rotation experiments) that address such possibilities.

We describe a system of large patches at the dorsal border of medial entorhinal cortex, which covers the entire mediolateral extent of medial entorhinal cortex and overlaps more medially with the parasubiculum (Caballero-Bleda and Witter, 1993). Because of their similarity and continuity with the parasubiculum, we suggest that the large dorsal patches should best be viewed as an extension of this structure. We note, however, that while previous authors described the parasubiculum as a multilayered structure (Witter and Amaral, 2004; Boccara et al., 2010), we found no evidence that the large dorsal patches were associated in any way with deep cortical layers. To our knowledge, the large dorsal patches have been largely unrecognized previously. Classically, the dorsal border of medial entorhinal cortex had been defined by the sudden increase in layer 2 width, which extends into layer 1 and forms a ''club-like thickening'' (Amaral and Witter, 1989; Insausti et al., 1997). Here, we provide several lines of evidence suggesting that this dorsal-most structure is organized in patches and contains a distinct neuronal subpopulation from the rest of medial entorhinal cortex. Cells in this structure have unique morphology and connectivity, are strongly theta modulated, show different theta-phase preferences, and are more head-direction selective than superficial layer neurons. In our study we assessed head-direction selectivity in an ''O''-shaped linear arena, and we cannot exclude that our directionality measures were influenced by the special geometry of this environment, in particular by the constraints imposed on the rat's heading direction. Nevertheless, under these experimental settings we could record head-direction cells, whose directional tuning was stable across clockwise and counterclockwise running directions and sharply tuned to a narrow angle (Figures 6I–6L; Figure S6). Further work is needed to extend these findings to open field environments, where spatial and head-directional modulation have been most extensively studied (Taube et al., 1990a; Taube and Muller, 1998; Sargolini et al., 2006). Consistent with our findings, head-direction cells have been recorded from the dorsal-most regions of medial entorhinal cortex in mice (Fyhn et al., 2008) and rats (Sargolini et al., 2006).

Theta rhythm is the most prominent oscillatory pattern in the hippocampal-entorhinal system and is thought to provide temporal windows for efficient neuronal communication (Dragoi and Buzsáki, 2006; Sirota et al., 2008; Mizuseki et al., 2009). In this respect, the timing of neuronal discharges relative to the underlying theta rhythm can provide important insights into the mechanisms that regulate temporal coordination within the network (Mizuseki et al., 2009). Interestingly, the spike-theta phase relationship was strikingly different between superficial layer and large patch cells. While the first appeared to fire preferentially on the ascending phase of the theta cycle (Figure 7F and 7G), large patch cells showed the strongest theta-phase locking and opposite theta-phase preferences from superficial layer cells, with maximal firing on the descending phase of the theta cycle, near the trough (Figures 7F and 7G; Figure S7A). Our data on the theta-phase preferences of layer 2 and 3 cells are consistent with recent findings (Hafting et al., 2008) but appear not to be in line with the work of Mizuseki et al. (2009). Several possibilities could account for the latter discrepancy, including our relatively small sample and the variability of theta-phase preferences among the layer 2 (Figure 7F; Figure S7A) and layer 3 populations (Mizuseki et al., 2009).

Our data confirm and extend previous observations on laminar differences in entorhinal cortex (Hafting et al., 2005; Sargolini et al., 2006). Our observations on a prevalence of spiny stellate morphologies and spatially modulated responses in layer 2 confirm previous morphological (Klink and Alonso, 1997) and physiological (Hafting et al., 2005; Sargolini et al., 2006) studies. Deep-layer neurons were largely silent during exploration. This result differs from the extracellular recording data of Sargolini et al. (2006), which indicated substantial deep-layer activity. We note, however, that most of the deep-layer cells recorded in our study were silent and could, therefore, not have been detected with extracellular recordings. Moreover, we used naive animals exploring a novel environment, whereas the recordings of Sargolini et al. (2006) were done in rats with prior spatial experience. Our results suggest that deep layers—and presumably also the hippocampal feedback that arrives in these layers (van Strien et al., 2009)—might not initially contribute to the representation of a novel environment.

In medial entorhinal cortex, position, speed, and directional information are integrated to generate an updated metric representation of space (McNaughton et al., 2006; Moser and Moser,

2008). In line with anatomical and structural features, like periodicities in cell densities, dendritic clusters (Ikeda et al., 1989), and molecular markers (Solodkin and Van Hoesen, 1996; Suzuki and Porteros, 2002), the patchy organization of medial entorhinal cortex further supports the existence of segregated functional modules, as previously suggested (Witter and Moser, 2006). This is in line with evidence that grid spacing and orientation are typically identical from grid cells recorded from the same location, while they change along the dorsoventral axis in a discontinuous fashion (Hafting et al., 2005; Fyhn et al., 2007; H. Stensland et al., 2010, Abstr. Soc. Neurosci., abstract). Interestingly, implementing an attractor-like modular organization within the grid cell network makes it possible to represent space in parallel at different spatial scales (Witter and Moser, 2006). In this context it is worth mentioning that indications for grid cell networks have been observed also in humans (Doeller et al., 2010), where the patchy organization of entorhinal cortex is most prominent (Hevner and Wong-Riley, 1992). The cytochrome oxidase-rich patches of entorhinal cortex are known to be destroyed in Alzheimer's disease (Solodkin and Van Hoesen, 1996), and we wonder if the destruction of patches is related to the loss of spatial orientation and awareness in Alzheimer's patients (Cherrier et al., 2001).

The localized connections between large patch cells and small patches suggest that each small patch might receive very selective and specific head-directional input for local computation. The focal head-directional input to small layer 2 patches is remarkable, since both our data and the results from previous studies (Sargolini et al., 2006) indicate that layer 2 cells express little or no head-direction selectivity. Therefore, since layer 2 cells do not simply inherit head-direction selectivity via centripetal axons, we wonder if head-directional information is transformed in layer 2 patches in a way that generates allocentric coding. More specifically, head-directional information could be used to generate allocentric coding by rotating (and thus allocentrically stabilizing) the grid pattern with head turns against egocentric coordinates. The circumcurrent axons form another prominent long-range circuit. We speculate that the circumcurrent axons might impose a global constraint that unifies directional information across large patch neurons to a single head direction.

Our work shows that in medial entorhinal cortex, cell identity strongly predicts both neuronal connectivity and physiology. We conclude that microcircuit analysis in behaving animals is both feasible and decisive for understanding the neural basis of spatial representations.

EXPERIMENTAL PROCEDURES

Juxtacellular Recording and Labeling of Single Neurons in Freely Moving Animals

Juxtacellular recording and labeling of single neurons were performed in freely moving Wistar rats (~P30–P50). Pipettes (4–6 MΩ) were filled with a solution containing NaCl 135 mM, KCl 5.4 mM, HEPES 5 mM, $CaCl_2$ 1.8 mM, and $MgCl_2$ 1 mM (pH 7.2) as well as biocytin (2%–3%). Standard surgical preparation, pipette anchoring, and anesthesia/wake-up procedures were performed as described previously (Lee et al., 2009). For targeting of the medial entorhinal cortex (left hemisphere), a small craniotomy (~2–4 mm diameter) was made 0.2–0.8 mm anterior to the transverse sinus and 4.5–5 mm lateral to the midline (Fyhn et al., 2008; Derdikman et al., 2009). Details are provided in the Supplemental Experimental Procedures.

Histological Analysis

To reveal the morphology of juxtacellularly labeled cells, 100–150 μm thick brain slices were processed with the avidin-biotin-peroxidase method (Lee et al., 2006, 2009; Epsztein et al., 2010). Cytochrome oxidase and Nissl stainings were performed as described previously (Wong-Riley 1979; Brecht and Sakmann, 2002). For myelin stainings a variation of the gold-chloride protocol (Schmued 1990) was used. Details are provided in the Supplemental Experimental Procedures.

Data Analysis

To assess spatial modulation of spiking activity, space was discretized into pixels of 2.5 × 2.5 cm bins, and color-coded firing maps were plotted. Head-direction tuning was measured as the length of the average vector of the circular distribution of firing rates. The head-direction index of a cell was defined as the vector length divided by average firing rate across the circular distribution. Theta modulation of spiking activity was quantified by measuring the maximum of the autocorrelation function's power spectrum between 4 and 10 Hz. For spike-theta phase analysis, juxtacellular signals were band-pass filtered at 4–10 Hz, and a Hilbert transform was used to determine the instantaneous theta phase of the filtered theta wave (peaks = 0°, 360° and troughs = 180°). Then, each spike was assigned the theta phase of the Hilbert transform at the time of that spike. Details are provided in the Supplemental Experimental Procedures.

SUPPLEMENTAL INFORMATION

Supplemental Information includes Supplemental Experimental Procedures and eight figures and can be found with this article online at doi:10.1016/j.neuron.2011.04.003.

ACKNOWLEDGMENTS

We thank Alison Barth, Prateep Beed, Rajnish Rao, Dietmar Schmitz, John Tukker, and Jason Wolfe for comments on the manuscript, and Brigitte Geue, Carolin Mende, Mike Kunert, Undine Schneeweiß, and Arnold Stern for outstanding technical assistance. This work was supported by Neurocure, the Bernstein Center for Computational Neuroscience (BMBF) and Humboldt University, the EU Biotact-grant, and the Neuro-behavior ERC grant.

Accepted: April 4, 2011
Published: May 25, 2011

REFERENCES

Alonso, A., and García-Austt, E. (1987). Neuronal sources of theta rhythm in the entorhinal cortex of the rat. I. Laminar distribution of theta field potentials. Exp. Brain Res. *67*, 493–501.

Alonso, A., and Klink, R. (1993). Differential electroresponsiveness of stellate and pyramidal-like cells of medial entorhinal cortex layer II. J. Neurophysiol. *70*, 128–143.

Amaral, D.G., and Witter, M.P. (1989). The three-dimensional organization of the hippocampal formation: A review of anatomical data. Neuroscience *31*, 571–591.

Beed, P., Bendels, M.H., Wiegand, H.F., Leibold, C., Johenning, F.W., and Schmitz, D. (2010). Analysis of excitatory microcircuitry in the medial entorhinal cortex reveals cell-type-specific differences. Neuron *68*, 1059–1066.

Boccara, C.N., Sargolini, F., Thoresen, V.H., Solstad, T., Witter, M.P., Moser, E.I., and Moser, M.B. (2010). Grid cells in pre- and parasubiculum. Nat. Neurosci. *13*, 987–994.

Brecht, M., and Sakmann, B. (2002). Dynamic representation of whisker deflection by postsynaptic potentials in morphologically reconstructed spiny

stellate and pyramidal cells in the barrels and septa of layer 4 in rat somatosensory cortex. J. Physiol. *543*, 49–70.

Brun, V.H., Solstad, T., Kjelstrup, K.B., Fyhn, M., Witter, M.P., Moser, E.I., and Moser, M.B. (2008). Progressive increase in grid scale from dorsal to ventral medial entorhinal cortex. Hippocampus *18*, 1200–1212.

Burwell, R.D. (2000). The parahippocampal region: Corticocortical connectivity. Ann. N Y Acad. Sci. *911*, 25–42.

Caballero-Bleda, M., and Witter, M.P. (1993). Regional and laminar organization of projections from the presubiculum and parasubiculum to the entorhinal cortex: An anterograde tracing study in the rat. J. Comp. Neurol. *328*, 115–129.

Cherrier, M.M., Mendez, M., and Perryman, K. (2001). Route learning performance in Alzheimer disease patients. Neuropsychiatry Neuropsychol. Behav. Neurol. *14*, 159–168.

Chorev, E., Epsztein, J., Houweling, A.R., Lee, A.K., and Brecht, M. (2009). Electrophysiological recordings from behaving animals–going beyond spikes. Curr. Opin. Neurobiol. *19*, 513–519.

Chrobak, J.J., and Buzsáki, G. (1998). Gamma oscillations in the entorhinal cortex of the freely behaving rat. J. Neurosci. *18*, 388–398.

Derdikman, D., and Moser, E.I. (2010). A manifold of spatial maps in the brain. Trends Cogn. Sci. *14*, 561–569.

Derdikman, D., Whitlock, J.R., Tsao, A., Fyhn, M., Hafting, T., Moser, M.B., and Moser, E.I. (2009). Fragmentation of grid cell maps in a multicompartment environment. Nat. Neurosci. *12*, 1325–1332.

Doeller, C.F., Barry, C., and Burgess, N. (2010). Evidence for grid cells in a human memory network. Nature *463*, 657–661.

Dragoi, G., and Buzsáki, G. (2006). Temporal encoding of place sequences by hippocampal cell assemblies. Neuron *50*, 145–157.

Epsztein, J., Lee, A.K., Chorev, E., and Brecht, M. (2010). Impact of Spikelets on Hippocampal CA1 Pyramidal Cell Activity During Spatial Exploration. Science *327*, 474–477.

Fyhn, M., Hafting, T., Treves, A., Moser, M.B., and Moser, E.I. (2007). Hippocampal remapping and grid realignment in entorhinal cortex. Nature *446*, 190–194.

Fyhn, M., Hafting, T., Witter, M.P., Moser, E.I., and Moser, M.B. (2008). Grid cells in mice. Hippocampus *18*, 1230–1238.

Hafting, T., Fyhn, M., Molden, S., Moser, M.B., and Moser, E.I. (2005). Microstructure of a spatial map in the entorhinal cortex. Nature *436*, 801–806.

Hafting, T., Fyhn, M., Bonnevie, T., Moser, M.B., and Moser, E.I. (2008). Hippocampus-independent phase precession in entorhinal grid cells. Nature *453*, 1248–1252.

Hevner, R.F., and Wong-Riley, M.T. (1992). Entorhinal cortex of the human, monkey, and rat: Metabolic map as revealed by cytochrome oxidase. J. Comp. Neurol. *326*, 451–469.

Houweling, A.R., and Brecht, M. (2008). Behavioural report of single neuron stimulation in somatosensory cortex. Nature *451*, 65–68.

Houweling, A.R., Doron, G., Voigt, B.C., Herfst, L.J., and Brecht, M. (2010). Nanostimulation: Manipulation of single neuron activity by juxtacellular current injection. J. Neurophysiol. *103*, 1696–1704.

Ikeda, J., Mori, K., Oka, S., and Watanbe, Y. (1989). A columnar arrangement of dendritic processes of entorhinal cortex neurons revealed by a monoclonal antibody. Brain Res. *505*, 176–179.

Insausti, R., Herrero, M.T., and Witter, M.P. (1997). Entorhinal cortex of the rat: Cytoarchitectonic subdivisions and the origin and distribution of cortical efferents. Hippocampus *7*, 146–183.

Klingler, J. (1948) Die Makroskopische Anatomie der Ammosformation. Denkschriften der Schweizerischen Natursforschenden Gesellschaft, Band 78., Abh. 1 (Zürich: Fretz).

Klink, R., and Alonso, A. (1997). Morphological characteristics of layer II projection neurons in the rat medial entorhinal cortex. Hippocampus *7*, 571–583.

Köhler, C. (1984). Morphological details of the projection from the presubiculum to the entorhinal area as shown with the novel PHA-L immunohistochemical tracing method in the rat. Neurosci. Lett. *45*, 285–290.

Langston, R.F., Ainge, J.A., Couey, J.J., Canto, C.B., Bjerknes, T.L., Witter, M.P., Moser, E.I., and Moser, M.B. (2010). Development of the spatial representation system in the rat. Science *328*, 1576–1580.

Lee, A.K., Manns, I.D., Sakmann, B., and Brecht, M. (2006). Whole-cell recordings in freely moving rats. Neuron *51*, 399–407.

Lee, A.K., Epsztein, J., and Brecht, M. (2009). Head-anchored whole-cell recordings in freely moving rats. Nat. Protoc. *4*, 385–392.

Lingenhöhl, K., and Finch, D.M. (1991). Morphological characterization of rat entorhinal neurons in vivo: Soma-dendritic structure and axonal domains. Exp. Brain Res. *84*, 57–74.

McNaughton, B.L., Battaglia, F.P., Jensen, O., Moser, E.I., and Moser, M.B. (2006). Path integration and the neural basis of the 'cognitive map'. Nat. Rev. Neurosci. *7*, 663–678.

Mizuseki, K., Sirota, A., Pastalkova, E., and Buzsáki, G. (2009). Theta oscillations provide temporal windows for local circuit computation in the entorhinal-hippocampal loop. Neuron *29*, 267–280.

Moser, E.I., and Moser, M.B. (2008). A metric for space. Hippocampus *18*, 1142–1156.

O'Keefe, J., and Dostrovsky, J. (1971). The hippocampus as a spatial map. Preliminary evidence from unit activity in the freely-moving rat. Brain Res. *34*, 171–175.

O'Keefe, J., and Nadel, L. (1978). The Hippocampus as a Cognitive Map (Oxford: Oxford University Press).

O'Keefe, J., and Burgess, N. (2005). Dual phase and rate coding in hippocampal place cells: Theoretical significance and relationship to entorhinal grid cells. Hippocampus *15*, 853–866.

Pinault, D. (1994). Golgi-like labeling of a single neuron recorded extracellularly. Neurosci. Lett. *170*, 255–260.

Pinault, D. (1996). A novel single-cell staining procedure performed in vivo under electrophysiological control: Morpho-functional features of juxtacellularly labeled thalamic cells and other central neurons with biocytin or Neurobiotin. J. Neurosci. Methods *65*, 113–136.

Quilichini, P., Sirota, A., and Buzsáki, G. (2010). Intrinsic circuit organization and theta-gamma oscillation dynamics in the entorhinal cortex of the rat. J. Neurosci. *30*, 11128–11142.

Sargolini, F., Fyhn, M., Hafting, T., McNaughton, B.L., Witter, M.P., Moser, M.B., and Moser, E.I. (2006). Conjunctive representation of position, direction, and velocity in entorhinal cortex. Science *312*, 758–762.

Schmued, L.C. (1990). A rapid, sensitive histochemical stain for myelin in frozen brain sections. J. Histochem. Cytochem. *38*, 717–720.

Shipley, M.T. (1974). Presubiculum afferents to the entorhinal area and the Papez circuit. Brain Res. *67*, 162–168.

Shipley, M.T. (1975). The topographical and laminar organization of the presubiculum's projection to the ipsi- and contralateral entorhinal cortex in the guinea pig. J. Comp. Neurol. *160*, 127–145.

Sirota, A., Montgomery, S., Fujisawa, S., Isomura, Y., Zugaro, M., and Buzsáki, G. (2008). Entrainment of neocortical neurons and gamma oscillations by the hippocampal theta rhythm. Neuron *60*, 683–697.

Solodkin, A., and Van Hoesen, G.W. (1996). Entorhinal cortex modules of the human brain. J. Comp. Neurol. *365*, 610–617.

Solstad, T., Boccara, C.N., Kropff, E., Moser, M.B., and Moser, E.I. (2008). Representation of geometric borders in the entorhinal cortex. Science *322*, 1865–1868.

Suzuki, W.A., and Porteros, A. (2002). Distribution of calbindin D-28k in the entorhinal, perirhinal, and parahippocampal cortices of the macaque monkey. J. Comp. Neurol. *451*, 392–412.

Suzuki, W.A., and Amaral, D.G. (2004). Functional neuroanatomy of the medial temporal lobe memory system. Cortex *40*, 220–222.

Taube, J.S. (2007). The head direction signal: Origins and sensory-motor integration. Annu. Rev. Neurosci. *30*, 181–207.

Taube, J.S., and Muller, R.U. (1998). Comparison of head direction cell activity in the postsubiculum and anterior thalamus of freely moving rats. Hippocampus *8*, 87–108.

Taube, J.S., Muller, R.U., and Ranck, J.B., Jr. (1990a). Head-direction cells recorded from the postsubiculum in freely moving rats. I. Description and quantitative analysis. J. Neurosci. *10*, 420–435.

Taube, J.S., Muller, R.U., and Ranck, J.B., Jr. (1990b). Head-direction cells recorded from the postsubiculum in freely moving rats. II. Effects of environmental manipulations. J. Neurosci. *10*, 436–447.

van der Linden, S., and Lopes da Silva, F.H. (1998). Comparison of the electrophysiology and morphology of layers III and II neurons of the rat medial entorhinal cortex in vitro. Eur. J. Neurosci. *10*, 1479–1489.

van Strien, N.M., Cappaert, N.L., and Witter, M.P. (2009). The anatomy of memory: An interactive overview of the parahippocampal-hippocampal network. Nat. Rev. Neurosci. *10*, 272–282.

Voigt, B.C., Brecht, M., and Houweling, A.R. (2008). Behavioral detectability of single-cell stimulation in the ventral posterior medial nucleus of the thalamus. J. Neurosci. *28*, 12362–12367.

Wills, T.J., Cacucci, F., Burgess, N., and O'Keefe, J. (2010). Development of the hippocampal cognitive map in preweanling rats. Science *328*, 1573–1576.

Witter, M.P., and Amaral, D.G. (2004). Hippocampal formation. In The Rat Nervous System, Third Edition, G. Paxinos, ed. (San Diego, CA: Academic Press), pp. 637–703.

Witter, M.P., and Moser, E.I. (2006). Spatial representation and the architecture of the entorhinal cortex. Trends Neurosci. *29*, 671–678.

Wong-Riley, M. (1979). Changes in the visual system of monocularly sutured or enucleated cats demonstrable with cytochrome oxidase. Brain Res. *171*, 11–28.

Wong-Riley, M.T. (1989). Cytochrome oxidase: An endogenous metabolic marker for neuronal activity. Trends Neurosci. *12*, 94–101.

Wong-Riley, M.T., Nie, F., Hevner, R.F., and Liu, S. (1998). Brain cytochrome oxidase. Functional significance and bigenomic regulation in the CNS. In Cytochrome Oxidase in Neuronal Metabolism and Alzheimer's Disease, F. Gonzalez-Lima, ed. (New York: Plenum Press), pp. 1–53.